Simulation of Semiconductor Processes and Devices 2016
Edited by E. Bär, J. Lorenz, and P. Pichler

Numerical Investigation of Junctionless Nanowire Transistors Using A Boltzmann/Schrödinger/Poisson Full Newton-Raphson Solver

Maziar Noei, Christoph Jungemann
Chair of Electromagnetic Theory
RWTH Aachen University
Aachen 52056, Germany
Email: mn@ithe.rwth-aachen.de

***Abstract*—A deterministic approach for solving the Poisson, Schrödinger and Boltzmann equations in 3D nanoscale devices is presented for the first time, where the Schrödinger equation is included via first order perturbation theory in the Newton-Raphson scheme. The developed solver is shown to be stable even in deep subthreshold simulations, and can provide insight in key phenomena occuring in ultra-short devices with confinement in two spatial dimensions.**

I. Introduction

In recent years, the deterministic approach to the Boltzmann transport equation (BTE) has evolved into a useful alternative to the stochastic Monte Carlo method. In this regard, many works have focused on self-consistently solving the coupled system of Poisson, Schrödinger, and Boltzmann equations [1], [2]. While all these works have used Gummel type iteration schemes, it is well-known that a full Newton-Raphson (FNR) method is superior in its convergence behavior and total solver time, and also paves the way towards small-signal and noise analyses. Concentrating on the Boltzmann/Schrödinger/Poisson system of equations, in 2013 Ruić *et al.* presented the first (and to date the only) FNR solver applicable to 2D devices that are translation invariant in their third spatial dimension [3]. However, a great variety of recent electronic devices are not translation invariant in their transverse direction and have to be treated in 3D. Following the main ideas in Ref. [3], we have extended the simulation domain to 3D devices and present a fully-coupled Poisson/Schrödinger/Boltzmann FNR solver applicable to devices with confinement in two dimensions.

This paper is organized as follows: after this short introduction, section II aims to explain in more detail the numerical schemes employed in our FNR solver. We then validate our solver by presenting and discussing the results of simulations in section III. The used framework allows to extract device properties such as transfer-characteristics, subthreshold-slope and DIBL and a look at the scaling behavior of the device directly based on physical models. Conclusions are finally drawn in section IV.

978-1-5090-0818-6/16/$31.00

II. Model

Figure 1 shows a $x-z$ cross section of the simulated device, which is an ultra-short radially-symmetric nanowire MOSFET. The z direction is the transport (longitudinal) direction and x, y the transverse directions. The Poisson equation is solved for the electrostatic potential in the 3D real space, the Schrödinger equation for each transverse cross section along the longitudinal axis, and the BTE for each subband in transport direction.

In what follows, we go through the details of our formulation and briefly explain how to incorporate the three constituent equations into an FNR solver. Different functions' domains of interest are omitted for better readability.

A. Schrödinger equation

In order to model the effects of quantum confinement, we solve the time-independent Schrödinger equation in $x-y$ slices perpendicular to the transport direction and obtain 1D subbands for electrons:

$$\Big[-\frac{\hbar^2}{2}\nabla_{xy}\cdot(\mathbf{m}_{\nu,\perp}^{-1}\nabla_{xy})-q\varphi(\mathbf{r})\Big]\psi^{\nu}(\mathbf{r})=\varepsilon^{\nu}(z)\psi^{\nu}(\mathbf{r}) \quad (1)$$

with $\mathbf{m}_{\nu,\perp}$ being the valley-dependent effective mass tensor in the transverse plane and q the positive electron charge. $\varepsilon^{\nu}(z)$ is the resulting energy eigenvalue and $\psi^{\nu}(\mathbf{r})$ is the corresponding wavefunction. $\nu=(v,s)$ captures both the valley index and the subband index.

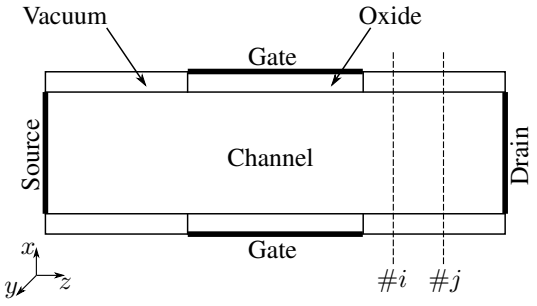

Fig. 1. Schematic drawing of the $x-z$ cross section of a gate-all-around junctionless nanowire transistor with a silicon channel.

B. Poisson equation

The potential in the 3D simulation domain obeys the Poisson equation:

$$\nabla_{\mathbf{r}} \cdot \big[\kappa(\mathbf{r})\nabla_{\mathbf{r}}\varphi(\mathbf{r})\big] = q\big[n(\mathbf{r}) - N_D(\mathbf{r})\big] \tag{2}$$

where $\varphi(\mathbf{r})$ is the electrostatic potential, $n(\mathbf{r})$ is the electron concentration, $N_D(\mathbf{r})$ is the donor concentration, and $\kappa(\mathbf{r})$ is the isotropic dielectric constant.

Equation (2) is solved for an unstructured triangular grid using the finite volume method, which guarantees flux conservation. Discretization leads to a set of equations with a structure as,

$$F_{\text{PE}} := \mathcal{P}_{\text{Lin}}(\varphi) + \mathcal{P}_{\text{Ch}}(f;\varepsilon,\psi) = 0 \tag{3}$$

where $\mathcal{P}_{\text{Lin}}$ represents the discretization of the differential operators and has a linear dependency on the electrostatic potential. The second term $\mathcal{P}_{\text{Ch}}$, on the other hand, contains the charge density and hence represents a direct feedback from BTE into PE. The electron density is calculated as:

$$n(\mathbf{r}) = 2\sum_{\nu}\left(\int_{\varepsilon^{\nu}(z)}^{\infty} Z^{\nu}(z,H) f^{\nu}(z,H)dH\right)|\psi^{\nu}(\mathbf{r})|^2 \tag{4}$$

where $Z^{\nu}(z,H)$ is the 1D DOS, and the subband energies are the lower bounds of integration in the H-transformed energy space.

C. Boltzmann equation

The stationary BTE with its 1D k-space reads:

$$v(k_z)\frac{\partial}{\partial z}f^{\nu}(z,k_z) + \frac{1}{\hbar}F(z)\frac{\partial}{\partial k_z}f^{\nu}(z,k_z) - S\{f\} = 0 \tag{5}$$

where $F(z)$ and $v(k_z)$ are the force and group velocity in transport direction, respectively. $S\{f\}$ is the scattering integral.

The choice of the discretization scheme strongly influences the numerical performance and stability of the solver. In this work, we have used the so-called H-transformation for which (5) is formulated in the total energy H [4]. This transformation removes the derivative w.r.t. k_z and the BTE changes into a first order partial differential equation only in z, with the total energy merely acting as a parameter. With the H-transformation, we immediately get the advantage of having a grid which is aligned with the trajectories of ballistic carriers. This implies that the equation can be easily stabilized by introducing a staggered grid and splitting the distribution function into its even/odd parts. An odd-elimination process results in matrices which have property M. This, however, comes at a certain cost: the total energy grid must be aligned with the subband energy profiles, and the detailed dependence of electron velocity, DOS and scattering rates on subband minima must be carefully taken into consideration. After the box integration, we get the following structure for the BTE:

$$F_{\text{BTE}} := \mathcal{B}_{\text{Fr}}(f;\varepsilon) + \mathcal{B}_{\text{Sc}}(f;\varepsilon,\psi) = 0 \tag{6}$$

where $\mathcal{B}_{\text{Fr}}$ and $\mathcal{B}_{\text{Sc}}$ represent the free-streaming and scattering terms, respectively. These terms implicitly depend on the electrostatic potential through ε^{ν} and ψ^{ν}, which are obtained from the Schrödinger equation.

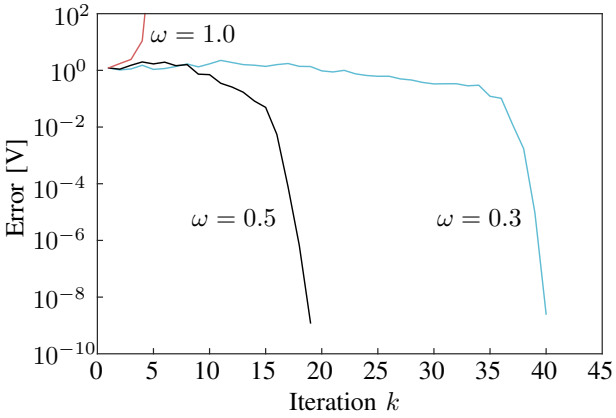

Fig. 2. Convergence behavior of our FNR solver for different damping factors. The damping is turned off when the error is less than 10^{-1}.

Regarding the scattering term, different types of scattering processes are characterized by their respective transition rates. The inter-valley transition rate reads [5]:

$$S_{\eta,\nu'\nu}(\vec{k}'|\vec{k}) = \frac{\pi\left(D_t K_\eta\right)^2}{\Omega\rho\omega_\eta} F^{\nu\nu'}\left(n(\hbar\omega_\eta) + \frac{1}{2} \pm \frac{1}{2}\right) \delta\left(\varepsilon_{\nu'}(\vec{k}') - \varepsilon_{\nu}(\vec{k}) \pm \hbar\omega_\eta\right) r(\eta,\nu(\vec{k}'),\nu(\vec{k})) \tag{7}$$

where ρ is the mass density, $D_t K_\eta$ the coupling constant, ω_η the phonon frequency, and r the selection rule of the phonon mode η. The occupation number for the phonons is given by the Bose-Einstein distribution. The intra-valley acoustic phonon scattering is approximated as an elastic process, and treated within the deformation potential theory [5]:

$$S_{\nu'\nu}(\vec{k}'|\vec{k}) = \frac{2\pi(k_{\text{B}}T_{\text{L}})\Xi^2}{\hbar\rho u_l^2} F^{\nu\nu'}\,\delta(v - v') \tag{8}$$

Ξ is the deformation potential and u_l is the longitudinal sound velocity. $F_{\nu\nu'}$ represents the overlap integral, and is given by:

$$F^{\nu\nu'} = \int dxdy|\psi^{\nu}(x,y)|^2\;|\psi^{\nu'}(x,y)|^2\;. \tag{9}$$

D. Full Newton-Raphson method

The coupled Boltzmann, Poisson, and Schrödinger equations are solved by the Newton-Raphson scheme, with the unknown variables being $\varphi(\mathbf{r})$ and $f^{\nu}(z,H)$. The dependency on electrostatic potential is considered implicitly in the electron density with $\varepsilon^{\nu}(z)$ and $\psi^{\nu}(\vec{r})$, which represent a direct feedback from the Schrödinger equation to the Poisson equation.

The Schrödinger equation, being an eigenvalue problem, cannot be directly cast into the FNR matrix equation. However, we can use the first order time-independent perturbation theory in order to express the changes in ε^{ν} and ψ^{ν} in terms of

changes in electrostatic potential and calculate the corresponding derivatives [6]. The first order correction to the subband energies and wavefunctions due to a small perturbation $\delta\varphi$ for the non-degenerate case is:

$$\delta\varepsilon^{\nu}(z) = -q \int d\mathbf{r}' |\psi^{\nu}(\mathbf{r}')|^2 \delta\varphi(\mathbf{r}) \delta(z' - z) \tag{10}$$

$$\delta\psi^{\nu}(\mathbf{r}) = -q \sum_{s' \neq s} \frac{\int d\mathbf{r}' \psi^{\nu'}(\mathbf{r}') \delta\varphi(\mathbf{r}) \psi^{\nu'}(\mathbf{r}')}{\varepsilon^{\nu}(z) - \varepsilon^{\nu'}(z)} \psi^{\nu'}(\mathbf{r}') \delta(z' - z) \tag{11}$$

Linearization of the three equations gives:

$$F_{\mathrm{PE}} = \left(\frac{\partial \mathcal{P}_{\mathrm{Lin}}}{\partial \varphi} + \frac{\partial \mathcal{P}_{\mathrm{Ch}}}{\partial \varepsilon} \frac{\partial \varepsilon}{\partial \varphi} + \frac{\partial \mathcal{P}_{\mathrm{Ch}}}{\partial \psi} \frac{\partial \psi}{\partial \varphi} \right) \delta\varphi + \frac{\partial \mathcal{P}_{\mathrm{Ch}}}{\partial f} \delta f \tag{12}$$

$$F_{\mathrm{BTE}} = \left(\frac{\partial \mathcal{B}_{\mathrm{Fr}}}{\partial \varepsilon} \frac{\partial \varepsilon}{\partial \varphi} + \frac{\partial \mathcal{B}_{\mathrm{Sc}}}{\partial \varepsilon} \frac{\partial \varepsilon}{\partial \varphi} + \frac{\partial \mathcal{B}_{\mathrm{Sc}}}{\partial \psi} \frac{\partial \psi}{\partial \varphi} \right) \delta\varphi + \left(\frac{\partial \mathcal{B}_{\mathrm{Fr}}}{\partial f} + \frac{\partial \mathcal{B}_{\mathrm{Sc}}}{\partial f} \right) \delta f \tag{13}$$

which can now be incorporated into the FNR solver.

In order to avoid divergence in the first few iterations, we can either use a Gummel type iteration up to a predefined threshold and then start the FNR solver, or we can use a damping factor in the first iterations of the FNR scheme. Figure 2 demonstrates the influence of a damping factor on the convergence behavior. As expected, while having a damping factor helps in solving the FNR equations in otherwise divergent cases, choosing a too small potential update might also result in an unnecessary long simulation time. Therefore, a reasonable value for ω has to be chosen for each simulation.

III. Results

In this section we demonstrate the features of our solver by simulating ultra-short radially-symmetric nanowire MOSFETs. The source/drain n^+ regions are 10nm long each, with doping concentration of $N_D^+ = 2 \times 10^{19}\mathrm{cm}^{-3}$. The channel region is doped to $N_D = 1 \times 10^{14}\mathrm{cm}^{-3}$. Potential and electron density for different gate biases are shown in Fig. 3 along the symmetry line (z axis) of the device. We can see that the deterministic simulation in H-space is numerical robust and produces very smooth results over more than 10 decades of magnitude. Such deep subthreshold simulations are practically impossible with Monte Carlo methods.

Figure. 4 shows the calculated $I_{\mathrm{DS}} - V_{\mathrm{DS}}$ characteristics for different V_{GS} values. An abnormal kink is evident in the results, which shifts to higher V_{DS} values for higher gate voltages. This kink vanishes in the ballistic limit, and is caused by elastic scattering when V_{DS} is such that the maximum of the electron distribution in the first subband is energetically aligned with the bottom of the second subband near the drain end of the device. This effect is discussed in more detail by Fischetti *et al.* [2].

Next, the device characteristics have been investigated as a function of channel length, with L_{ch} ranging from 5nm to 90nm. Looking at Fig. 5 and Fig. 6, it is evident that while the output current is larger for shorter channel lengths due to the proportionality of channel resistance and channel length, the device loses a great deal in performance in terms of its subthreshold slope and output resistance. With $L_{\mathrm{ch}} < 10$ nm, the gate's electrostatic control is not sufficient to keep the subthreshold swing at the theoretical minimum. The subthresh-

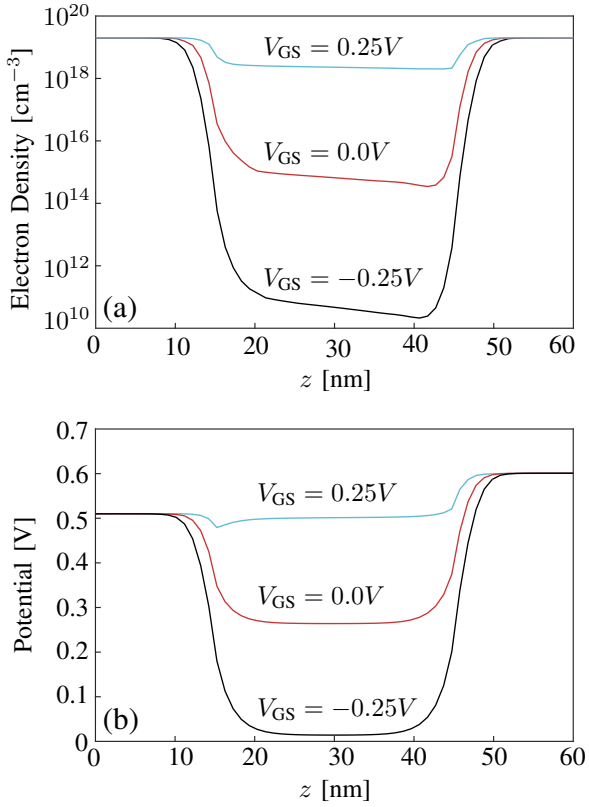

Fig. 3. (a) Electron density, and (b) electrostatic potential in the transport direction for different gate voltages. The values are plotted at the center of nanowire. The channel length is $L_{\mathrm{ch}} = 28$ nm.

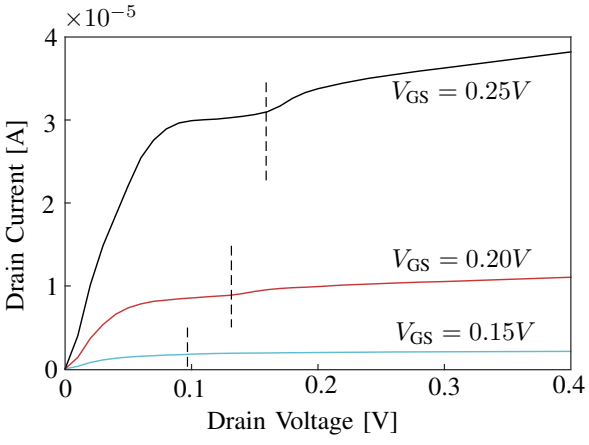

Fig. 4. $I_{\mathrm{DS}} - V_{\mathrm{DS}}$ curves of the transistor at different gate biases. The channel length is $L_{\mathrm{ch}} = 28$ nm.

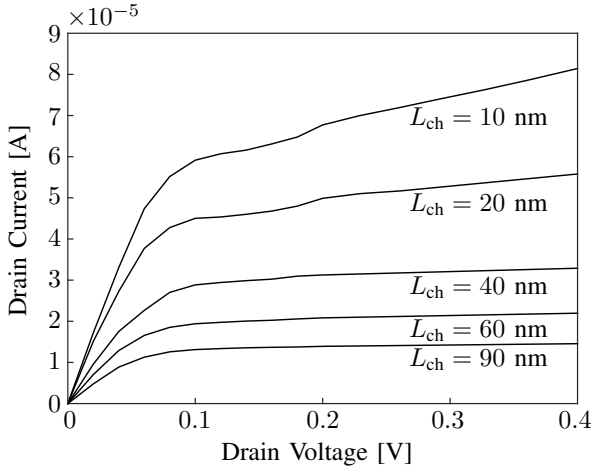

Fig. 5. Output characteristics of the simulated transistor for different channel lengths at $V_{GS} = 0.25V$.

old swing, however, remains approximately constant beyond $L_{ch} = 10$ nm.

Finally, the scaling behavior of the simulated silicon nanowire MOSFET in terms of its on-current I_{on}, off-current I_{off}, and I_{on}/I_{off} ratio is presented in Fig. 7. The on-current is measured at $V_{GS} = 0.25V$ and the off-current at $V_{GS} = -0.25V$, both with $V_{DS} = 0.4V$. Again, the device's performance deteriorates as we scale the channel length below $15 - 20$ nm.

IV. Conclusion

We have developed a quadratically converging stable FNR solver for the combined system of Poisson, Schrödinger and Boltzmann equations which can be used for numerical investigations of nanowire transistors. The FNR approach is superior to the Gummel type iteration schemes in convergence behavior and total solver time. In order to demonstrate the features of the FNR solver, ultra-short radially-symmetric silicon nanowire MOSFETs were simulated. We extracted

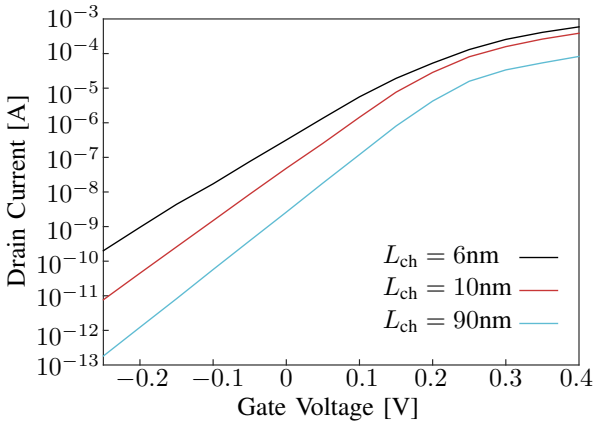

Fig. 6. $I_{DS} - V_{GS}$ characteristics of the simulated transistor for different channel lengths at $V_{DS} = 0.4V$.

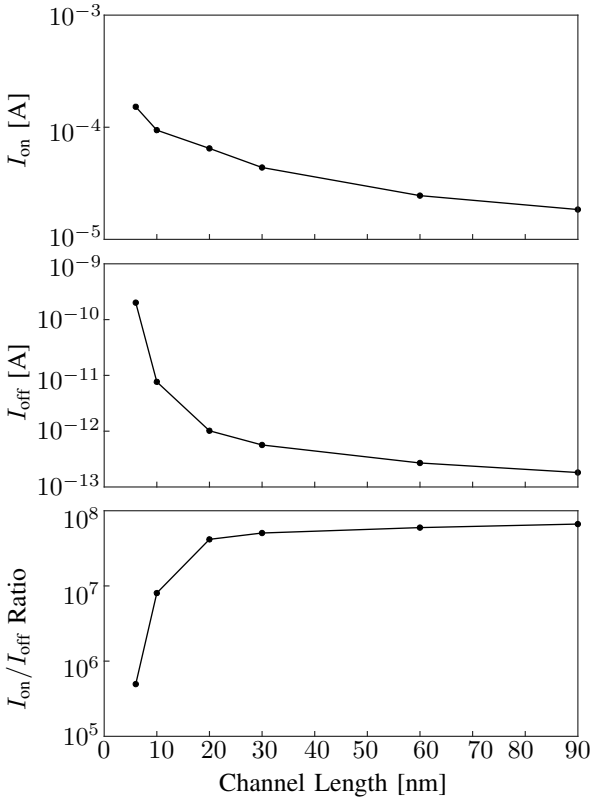

Fig. 7. On-current, off-current, and on/off current ratio for different channel lengths. Simulations are performed for $V_{DS} = 0.4V$ and $V_{GS} = \pm 0.25V$.

the deep subthreshold characteristics of these devices, which cannot be easily extracted by Monte Carlo methods. We also investigated the scaling behavior of the nanowire transistors, noting that such studies would be much more expensive if we were to use other methods such as the NEGF formalism.

References

[1] S. Scaldaferri, G. Curatola, and G. Iannaccone, "Direct solution of the boltzmann transport equation and poisson/schrödinger equation for nanoscale mosfets," vol. 54, no. 11, 2007.

[2] S. Jin, M. V. Fischetti, and T. w. Tang, "Theoretical study of carrier transport in silicon nanowire transistors based on the multisubband Boltzmann transport equation," *Electron Devices, IEEE Transactions on*, vol. 55, pp. 2886–2897, 2008.

[3] D. Ruić and C. Jungemann, "A self-consistent solution of the Poisson, Schrödinger and Boltzmann equations by a full Newton-Raphson approach for nanoscale semiconductor devices," in *Simulation of Semiconductor Processes and Devices (SISPAD), 2013 International Conference on*, pp. 356–359, Sept 2013.

[4] S.-M. Hong, A. T. Pham, and C. Jungemann, *Deterministic solvers for the Boltzmann transport equation*. Computational Microelectronics, Wien, New York: Springer, 2011.

[5] C. Jungemann and B. Meinerzhagen, *Hierarchical Device Simulation: The Monte-Carlo Perspective*. Computational Microelectronics, Wien, New York: Springer, 2003.

[6] R. Shankar, *Principles of quantum mechanics*. New York: Springer, 1994.